https://doi.org/10.5194/wes-2025-206
Preprint. Discussion started: 21 November 2025
© Author(s) 2025. CC BY 4.0 License.

eawe european academy of wind energy
Open Access WIND ENERGY SCIENCE DISCUSSIONS

Wind speed estimation using second-order sliding-mode observers: simulation and experimental validation on a floating offshore wind turbine

Moein Sarbandi[1], Matis Viozelange[1], Mohamed Assaad Hamida[1], and Franck Plestan[1]
[1]Nantes Université, École Centrale Nantes, CNRS, LS2N, UMR 6004, Nantes, F-44000, France
Correspondence: Moein Sarbandi (moein.sarbandi@ec-nantes.fr)

Abstract. Wind speed estimation is crucial for the control and performance optimization of floating offshore wind turbines (FOWTs). This paper introduces a robust estimation framework based on second-order sliding-mode observers (SOSMOs), developed in both constant-gain and adaptive versions. The observers are developed using a reduced-order dynamic model and validated in the OpenFAST simulation environment when all degrees of freedom are activated. Their performances are compared with the continuous-discrete extended Kalman filter (CD-EKF) used in the reference open-source controller (ROSCO). The proposed approach is assessed under stochastic wind/wave conditions through OpenFAST simulations and further validated experimentally using a scaled software-in-the-loop (SIL) setup. Simulation results indicate that the proposed observers perform comparably to the CD-EKF in terms of estimation accuracy, while offering robustness, simpler implementation, and reduced computational complexity.

1 Introduction

The increasing global demand for electricity has necessitated the exploration of sustainable energy solutions, with offshore wind energy emerging as a key contributor. Floating offshore wind turbines (FOWTs) offer access to vast, underutilized wind resources located in deep waters, which account for approximately 80 % of the global offshore wind potential, as reported by (Global Wind Energy Council, 2022). Compared with fixed-bottom turbines, FOWTs benefit from stronger and more consistent winds; however, the floating structure introduces additional degrees of freedom, such as platform motions, which can cause negative damping and exacerbate power fluctuations. In extreme cases, this instability could lead to system failure. Consequently, conventional strategies developed for onshore wind turbines are not sufficiently effective for floating ones. Therefore, advanced estimation and monitoring approaches are required to support the stability and efficiency of FOWTs (McCoy et al., 2024; Stockhouse et al., 2024).

The operation of wind turbines is typically divided into four regions based on the prevailing wind speed (Stockhouse et al., 2024). In Region I (below the cut-in wind speed), the turbine sits idle waiting for the wind speed to increase, as the available wind energy is insufficient to operate the turbine. In Region IV (above the cut-out wind speed), the turbine also stops operating to prevent potential damage. In contrast, power generation occurs in Region II and Region III, each employing distinct control strategies. In Region II, the objective is to maximize the power coefficient to optimize energy capture whereas in Region III,

https://doi.org/10.5194/wes-2025-206
Preprint. Discussion started: 21 November 2025
© Author(s) 2025. CC BY 4.0 License.

eawe european academy of wind energy
Open Access WIND ENERGY SCIENCE DISCUSSIONS

the objective is to keep the power at its nominal value. Indeed, maintaining power at its rated level is essential to protect the turbine ensure its longevity and operational stability.

In the operation of FOWTs, accurate information about wind speed is a fundamental requirement for control system design, real-time monitoring, and ensuring the safe and efficient performance of the turbine (Soltani et al., 2013). Wind speed information serves multiple critical functions depending on the control strategy employed. For example, in Region II, wind speed is used to compute the optimal rotor speed reference based on the desired tip-speed ratio whereas in Region III, it plays a central role in blade pitch control action (Stockhouse et al., 2024). Furthermore, wind speed measurements are a key input for feed-forward control algorithms. The quality of wind speed information thus has a direct impact on the overall performance and longevity of FOWTs.

Different methods exist in the literature regarding wind speed measurement or estimation on FOWTs, including sensor-based, observer-based, and neural network-based approaches.

LiDAR use. An advanced sensor-based method commonly used for wind speed estimation is light detection and ranging (LiDAR) (Shu et al., 2016). A considerable amount of literature is using LiDAR such as (He et al., 2025; Moldenhauer and Schmid, 2025; Li and Geng, 2024; Mahdizadeh et al., 2021). Despite the widespread adoption of LiDAR systems for wind speed measurement, some disadvantages have to be mentioned. One of the most apparent limitations is the cost and the maintenance demand of these systems (Jena and Rajendran, 2015). LiDAR devices, particularly those used in offshore and floating structures, are expensive to acquire and install, and their operation in harsh marine environments imposes high standards on longevity, autonomous operation, and regular maintenance to guarantee data quality. In addition, a primary technical limitation lies in the vulnerability of LiDAR measurements to motion-induced errors. Floating platform motions distort the LiDAR's line of sight, introducing systematic biases and increased uncertainty in wind speed estimation (Gräfe et al., 2023). Such disturbances can lead to errors in real-time control. These limitations highlight the need for alternative or enhanced wind speed estimation techniques that are accurate, sensorless, and therefore more cost-effective.

Neural-networks based methods. Alternatively, some recent studies rely on neural network-based methods for wind speed estimation and forecasting (Zhang et al., 2024; Sierra-García and Santos, 2021; Pan et al., 2022). These methods typically require an offline training phase using large datasets that must accurately represent the system's operating conditions (Chen and Han, 2022). However, deep learning models behave like black boxes, offering limited interpretability and making it difficult to guarantee and formally prove stability or robustness of the closed-loop system. Additionally, the generalization of these models to unseen conditions remains a significant challenge.

Kalman filter solution. Another widely adopted alternative is the Kalman filter (KF) and its variants. In (Soltani et al., 2013), both linear and nonlinear KFs are used for wind speed estimation. The simulation results also showed that the performance of nonlinear KF is better than the other at the transient state for the reason that the time response of nonlinear KF is much smaller than that of linear KF. KFs provide model-based state estimation by integrating a system's dynamic equations with available sensor measurements. In wind turbine applications, they have been employed to estimate wind speed by combining turbine output data with linear aerodynamic models (Boukhezzar and Siguerdidjane, 2011). However, since wind turbine systems are inherently nonlinear, standard KFs do not perform well in dynamic operating conditions. To address this, extended Kalman

https://doi.org/10.5194/wes-2025-206
Preprint. Discussion started: 21 November 2025
© Author(s) 2025. CC BY 4.0 License.

eawe european academy of wind energy
Open Access WIND ENERGY SCIENCE DISCUSSIONS

filters (EKFs) have been developed to handle nonlinearities more effectively. A wind speed estimation method based on EKF was introduced in (Song et al., 2017) to improve the efficiency of wind turbine operation. By integrating this algorithm with optimal tip-speed ratio tracking, the study demonstrated enhanced control of maximum power output. This paper reported that the proposed method could raise annual energy output by around 0.8 %. In (Hernández et al., 2014), the application of an EKF for wind speed estimation was demonstrated using real experimental data. This study is particularly noteworthy, as it validates the reliability of the EKF-based estimation method with real-world operating data.

Furthermore, some studies, such as (Chen et al., 2025; Knudsen et al., 2011), use an indirect method for wind speed estimation. In these approaches, aerodynamic torque is first estimated, allowing then the estimation of wind speed. In (Kim et al., 2024), two methods of wind speed estimation are used and compared. The first one is based on the drive-train model using measured rotor speed, pitch angle, and generator torque as inputs, and the second one involves applying the estimated wind speed using a 3D look-up table and is compared with a continuous-discrete extended Kalman filter (CD-EKF).

Despite their widespread use, EKF-based methods for estimating wind speed have several limitations that restrict their applicability in FOWTs. One key challenge lies in the tuning of process and measurement noise covariance matrices, which is often heuristic and lacks a systematic procedure. Improper tuning can lead to divergence (Chen et al., 2025; Song et al., 2017). Additionally, EKFs require approximation of the model around operating points, making them sensitive to variations in system dynamics and reducing their accuracy in highly nonlinear or time-varying conditions. This is particularly problematic in FOWTs, where platform motions introduce significant nonlinearity. Furthermore, the EKF also suffers from poor robustness to model mismatch and unmodeled dynamics, which are common in offshore environments. Finally, the formal proof of stability of the closed-loop including KF/EKF solutions is not trivial. These drawbacks highlight the need for more robust, model-insensitive alternatives for wind speed estimation.

Observer based on sliding mode theory. Among observer-based approaches, sliding mode observers (SMOs) have attracted significant attention due to their inherent robustness to uncertainties and disturbances, which are particularly prevalent in offshore environments. Unlike KFs, which rely heavily on accurate statistical models and noise characteristics, SMOs exploit the system nonlinear structure and discontinuous logic to force estimation errors to converge in finite time (Ma et al., 2024). This makes them well-suited for FOWTs, where system dynamics are often poorly known and subject to unpredictable perturbations. Furthermore, recent studies have demonstrated the potential of higher-order sliding mode observers to achieve estimation even in the presence of uncertainties, while reducing the negative effect (chattering (Davila et al., 2005)) induced by discontinuity appearing in the correction term. For example, in (Barambones et al., 2021), the authors estimated aerodynamic torque to be used as a reference in calculating the turbine's optimal rotor speed for maximizing wind power capture.

Although numerous studies in the field of FOWTs assume perfect knowledge of wind speed, the current paper proposes the use of a second-order sliding mode observer (SOSMO) structure for wind speed estimation, applied to FOWTs. Furthermore, the proposed solution includes an adaptive second-order sliding mode observer (ASOSMO) that is a novelty in the context of wind turbines. Indeed, tuning SMOs/SOSMOs remains a persistent challenge, as it typically requires prior knowledge of the bounds of perturbations, the use of adaptation laws to evaluate the gain (as shown in (Plestan et al., 2010) for adaptive sliding mode control) allows to obtain very performant solutions requiring reduced tuning effort and limited knowledge of the model.

https://doi.org/10.5194/wes-2025-206
Preprint. Discussion started: 21 November 2025
© Author(s) 2025. CC BY 4.0 License.

eawe european academy of wind energy
Open Access WIND ENERGY SCIENCE DISCUSSIONS

It is important to notice that, in the sequel, a formal analysis of observability is made to verify that the wind estimation can be evaluated from the single measurement of the rotor speed; it is rarely made in the context of (FO)WTs.
In the sequel, the approach is validated through simulations using the National Renewable Energy Laboratory (NREL) 5 MW FOWT within the OpenFAST simulation framework (Jonkman et al., 2009), and its performance is compared with the CD-EKF implemented in the reference open-source controller (ROSCO) (Abbas et al., 2022). It is also evaluated on a software-in-the-loop located in LHEEA lab, Nantes, France and dedicated to reduced-scale model of a FOWT.

The **main contributions and original points** of the present paper are summarized as follows

- A numerical method for observability analysis is proposed by supposing that the estimated variable is the wind speed and the single measured variable is the rotor speed.
- Then, observers based on sliding mode theory are proposed for wind speed estimation, from a single measurement that is the rotor speed, and are compared to a CD-EKF used in ROSCO.
- Two SOSMOs are designed: a constant-gain structure and an adaptive-gain one (allowing dynamic tuning of the gain without any information on the system uncertainties and perturbations).
- The observers are developed using a reduced-order model but validated within the OpenFAST simulator when all degrees of freedom of the FOWT are activated.
- Experimental validation is conducted using a scaled software-in-the-loop (SIL) test setup replicating realistic wind and wave conditions.

This paper is organized as follows: Sect. 2 presents the reduced-order dynamic model of the FOWT; Sect. 3 develops the proposed SMOs, including observability analysis, observer formulation, and adaptive gain design; Sect. 4 reports simulation studies and comparative evaluations with the CD-EKF under different wind conditions; Sect. 5 describes the experimental validation using a SIL setup; and Sect. 6 concludes by summarizing the main findings and outlining directions for future research.

2 Observation-oriented model

The present study focuses on the NREL 5-MW FOWT OC4, which is supported by a semi-submersible floating platform and simulated using OpenFAST (Jonkman et al., 2009).

https://doi.org/10.5194/wes-2025-206
Preprint. Discussion started: 21 November 2025
© Author(s) 2025. CC BY 4.0 License.

eawe european academy of wind energy
Open Access WIND ENERGY SCIENCE DISCUSSIONS

2.1 Aerodynamic and drive-train modeling

Wind turbines harness the kinetic energy of the wind to generate mechanical power through aerodynamic interaction between the wind and the rotating blades. The theoretical power available in the wind stream is given by

$$P_{\text{wind}} = \frac{1}{2}\rho\pi R^2 v^3 \tag{1}$$

where ρ is the air density, R is the rotor radius, and v is the wind speed upstream of the rotor. However, only a portion of this energy can be converted into mechanical power owing to fundamental aerodynamic limits, such as Betz's law (Manwell et al., 2009). The efficiency of this conversion is described by the power coefficient C_p, which quantifies the fraction of the wind's kinetic energy that is captured by the rotor. As a consequence, aerodynamic power P_a and torque τ_a read as

$$P_a = \frac{1}{2}\rho\pi R^2 C_p\left(\lambda,\beta\right) v^3 \tag{2}$$

$$\tau_a = \frac{P_a}{\omega} \tag{3}$$

where ω is the rotor speed, and the power coefficient $C_p(\lambda,\beta)$ is a nonlinear function of the tip-speed ratio λ and the blade pitch angle β, as depicted in Fig. 1. The tip-speed ratio is defined as

$$\lambda = \frac{\omega R}{v} \tag{4}$$

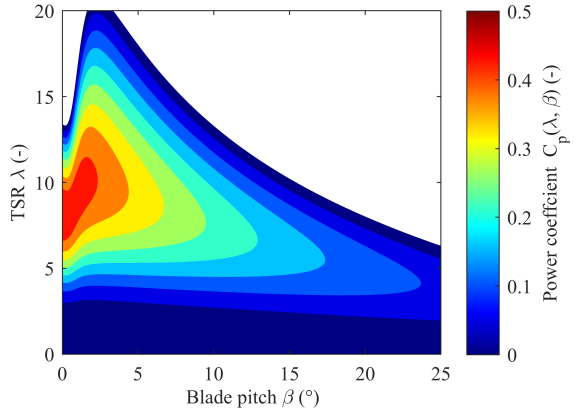

Figure 1. Power coefficient C_p with respect to tip-speed ratio λ and blade pitch angle β (Sarbandi et al., 2025).

2.2 Reduced-order observation-oriented model of a FOWT

The full-order FOWT model includes a high number of degrees of freedom (24), taking into account for blade and tower bending modes, platform pitch and surge motions, and mooring dynamics. While this comprehensive model captures detailed

https://doi.org/10.5194/wes-2025-206
Preprint. Discussion started: 21 November 2025
© Author(s) 2025. CC BY 4.0 License.

eawe european academy of wind energy
Open Access WIND ENERGY SCIENCE DISCUSSIONS

turbine behavior, its complexity makes it unsuitable for control design and real-time estimation. Therefore, a reduced-order model is used for observer development. The equation of motion for the rotor speed ω is given by

$$\dot{\omega} = \frac{1}{J}(\tau_a - n_g \tau_g) + \delta(t), \tag{5}$$

where J is the equivalent rotational inertia, τ_a and τ_g respectively denote the aerodynamic and generator torques, n_g is the gearbox ratio, and $\delta(\cdot)$ captures unmodeled dynamics and disturbances.

The control vector consists of the generator torque and the blade pitch angle $u = [\tau_g \ \beta]^\top$, the used input depending on the operating region (Aslmostafa et al., 2025). In Region II, control is primarily achieved by adjusting the generator torque τ_g, with blade pitch angle fixed at $\beta = 0$. In contrast, Region III control is dominated by blade pitch β actuation, with the generator torque τ_g held constant at its rated value, *i.e.*, $\tau_g = \tau_g^*$.

The objective in this paper is to design an observation solution allowing the estimation of the wind speed v from the measurement of the rotor speed ω. The wind speed is here viewed as a time-varying parameter whose dynamics is unknown that gives

$$\dot{v} = f_v(t), \tag{6}$$

$f_v(t)$ being an unknown bounded function. To summarize, the observer-based model reads as

$$\begin{bmatrix} \dot{\omega} \\ \dot{v} \end{bmatrix} = \underbrace{\begin{bmatrix} \frac{1}{J}\left(\frac{\rho \pi R^3 v^2}{2\lambda} C_p(\lambda,\beta) - n_g \tau_g\right) \\ 0 \end{bmatrix}}_{F(x,u)} + \underbrace{\begin{bmatrix} \delta(t) \\ f_v(t) \end{bmatrix}}_{\Delta(t)} \tag{7}$$

the objective being to estimate v from the measurement of ω in spite of $\Delta(\cdot)$. The system can be written in observation-oriented form

$$\begin{aligned} \dot{x} &= F(x,u) + \Delta(t) \\ y &= H(x) \end{aligned} \tag{8}$$

with $x = [\omega \ v]^\top$ the state vector, $H(x) = \omega$ the measured output and $u = [\tau_g \ \beta]^\top$.

Remark 1. *The modeling of $C_p(\lambda,\beta)$ has been intensively made (Castillo et al., 2023). In this study, an exponential model is used that approximates the power coefficient and reads as*

$$C_p(\lambda,\beta) \approx a(\lambda,\beta)\beta + b(\lambda,\beta), \tag{9}$$

where the coefficients a and b are defined as

$$\begin{aligned} a &= -c_0 c_2 \exp(-c_4 \lambda_1^{-1}), \\ b &= c_0(c_1 \lambda_1^{-1} - c_3)\exp(-c_4 \lambda_1^{-1}), \end{aligned} \tag{10}$$

https://doi.org/10.5194/wes-2025-206
Preprint. Discussion started: 21 November 2025
© Author(s) 2025. CC BY 4.0 License.

eawe european academy of wind energy
Open Access WIND ENERGY SCIENCE DISCUSSIONS

with

$$\lambda_1^{-1} = \frac{1}{\lambda + c_5\beta} - \frac{c_6}{\beta^3 + 1}$$

and $c_0 = 0.5$, $c_1 = 73.5$, $c_2 = 0.4$, $c_3 = 5$, $c_4 = 13.125$, $c_5 = 0.08$, $c_6 = 0.0035$. ■

Remark 2. *In the case of FOWT, platform motions and mooring dynamics are not taken into account in Eq.* (8)*. The proposed estimation methods in the paper are developed on this simplified system and can then be applied to floating (or not) offshore (or not) wind turbines. In the sequel, the observation solutions for estimating the wind speed* v *are validated by supposing that only the rotor speed* ω *is measured, and through two separate steps: first using the full-order OpenFAST simulator, and then the experimental setup. This two-stage evaluation emphasizes the observer's robustness versus simplification of the model.* ■

3 Supertwisting-based observer

Ideally, to achieve high performance in the state/parameter estimation, having an accurate model of the system is a key point. However, modeling the exact dynamics of FOWTs is highly challenging. Therefore, it is crucial to develop estimation methods that are sufficiently robust against system perturbations and modeling uncertainties. In this section, a robust observer based on the supertwisting algorithm (Levant, 1993) is presented for estimating wind speed by using rotor speed measurement; this observer is based on the reduced-order model presented in the previous section. Additionally, the novelty of the proposed estimation algorithm lies in the fact that the gains are dynamically adapted, allowing an easier tuning.

Assumption 1. *The wind speed* $v(t)$ *is assumed to be unmeasured and dynamically unknown. Nevertheless,* $v(t)$ *remains bounded and positive for all* $t \geq 0$*, such that*

$$0 < v(t) < V_{\max} \quad \forall t \geq 0, \tag{11}$$

where $V_{\max} > 0$ *is a constant that represents an upper bound within the turbine's operational regions.* ■

Given the uncertain nature of the system described in Eq. (8), an observer inspired from (Shtessel et al., 2014) is proposed. However, the first step is to analyze the observability of Eq. (8) in the operational domain, possibly detecting singularities.

3.1 Observability analysis

This section is detailing the numerical procedure for the analysis of the observability of the system in Eq. (8). Denote the operating domain $\mathcal{O} \subset \mathbb{R}^4$ in which $x = [\omega\, v]^\top$ and $u = [\tau_g\, \beta]^\top$ are physically evolving. All the results detailed in the rest of the paper are verified only in this domain.

Assumption 2. *The perturbation term* $\delta(t)$ *and its derivative are bounded. Furthermore,* $\delta(t)$ *has no influence on the system observability.* ■

Given the previous assumption, the observability analysis developed in the sequel is made for the system in Eq. (8) *without* perturbation, *i.e.* $\delta(t) = 0$. The generic observability analysis is defined as follows.

Definition 1. (Krener and Respondek, 1985) *Consider the system given by Eq.* (8) *with* $x = [\omega\ v]^\top$ *and* $u = [\tau_g\ \beta]^\top$ *evolving in the operating domain* $\mathcal{O}$ *and suppose Assumption 2 is fulfilled. Consider that* $\delta(t) = 0$*. The system formulated in Eq.* (8) *is*

https://doi.org/10.5194/wes-2025-206
Preprint. Discussion started: 21 November 2025
© Author(s) 2025. CC BY 4.0 License.

eawe european academy of wind energy
Open Access WIND ENERGY SCIENCE DISCUSSIONS

locally observable if

$$\Phi_{\delta(t)=0} = \begin{bmatrix} y \\ \dot{y} \end{bmatrix}_{\delta(t)=0} = \begin{bmatrix} \omega \\ \frac{1}{J}\left(\frac{\rho\pi R^3 v^2}{2\,\lambda(\omega,v)}\,C_p(\lambda(\omega,v),\beta) - n_g\tau_g\right) \end{bmatrix} \tag{12}$$

is a state coordinate transformation, i.e. $z = \Phi(\omega, v, \beta, \tau_g)$ *is invertible on* $\mathcal{O}$. ■

The previous property is evaluated if $\Phi_{\delta(t)=0}$ can be inverted that is a very hard task in practice. It is why the previous definition can be reformulated by the next equivalent one.

Definition 2. *Consider the system given by Eq.* (8) *with* $x = [\omega\ v]^\top$ *and* $u = [\tau_g\ \beta]^\top$ *evolving in the operating domain* $\mathcal{O}$ *and suppose Assumption 2 fulfilled. The system is said generically observable on* $\mathcal{O}$ *if*

$$\mathrm{Det}\left[\frac{\partial \Phi_{\delta(t)=0}}{\partial x}\right] \neq 0 \tag{13}$$

with

$$\Phi_{\delta(t)=0} = \begin{bmatrix} y \\ \dot{y} \end{bmatrix}_{\delta(t)=0} = \begin{bmatrix} \omega \\ \frac{1}{J}\left(\frac{\rho\pi R^3 v^2}{2\,\lambda(\omega,v)}\,C_p(\lambda(\omega,v),\beta) - n_g\tau_g\right) \end{bmatrix} \tag{14}$$

■

Applying Eq. (13) to Eq. (14), it is obvious that the first line of the Jacobian $\partial\Phi/\partial x$ equals $[1\ 0]$.

Observability condition. The system defined by Eq. (8) is locally observable if the following condition is fulfilled

$$\frac{\partial \dot{y}}{\partial v} \neq 0 \ \rightarrow\ \frac{\partial C_p}{\partial v}\cdot v + 3\,C_p(\lambda(\omega,v),\beta) \neq 0 \tag{15}$$

In the simulation sections, the previous condition in Eq. (15) will be numerically and experimentally evaluated in realistic operating conditions.

3.2 Observer design

Consider the system defined by Eq. (8) that is locally observable. As a consequence, the transformation

$$z = \begin{bmatrix} z_1 \\ z_2 \end{bmatrix} = \begin{bmatrix} y \\ \dot{y} \end{bmatrix} = \Phi(\omega, v, \beta, \tau_g) \tag{16}$$

is a state coordinate one, *i.e.* the state vector $[\omega\ v]^\top$ can be expressed as a function of z_1, z_2, τ_g and β, *i.e.*

$$x = \begin{bmatrix} \omega \\ v \end{bmatrix} = \Phi^{-1}(z_1, z_2, \beta, \tau_g) \tag{17}$$

Furthermore, from the state coordinate transformation given in Eq. (16), one gets

$$\begin{aligned} \dot{z}_1 &= z_2 \\ \dot{z}_2 &= \ddot{\omega} = \frac{\mathrm{d}}{\mathrm{d}t}\left[\frac{\rho\pi R^3 v^2}{2J\lambda}\,C_p(\lambda,\beta)\right] - \frac{n_g}{J}\,\dot{\tau}_g + \dot{\delta}(t) \end{aligned} \tag{18}$$

https://doi.org/10.5194/wes-2025-206
Preprint. Discussion started: 21 November 2025
© Author(s) 2025. CC BY 4.0 License.

eawe european academy of wind energy
Open Access WIND ENERGY SCIENCE DISCUSSIONS

that can be rewritten as

$$\dot{z} = \begin{bmatrix} \dot{z}_1 \\ \dot{z}_2 \end{bmatrix} = \underbrace{\begin{bmatrix} 0 & 1 \\ 0 & 0 \end{bmatrix}}_{A} z + \begin{bmatrix} 0 \\ \mathcal{F}(\cdot) \end{bmatrix} \tag{19}$$

with (replacing ω and β with the state coordinate transformation in Eq. (17))

$$\mathcal{F}(\cdot) = \frac{\mathrm{d}}{\mathrm{d}t}\left[\frac{\rho\pi R^3 v^2}{2J\lambda} C_p(\lambda,\beta)\right] - \frac{n_g}{J}\dot{\tau}_g + \dot{\delta}(t) \tag{20}$$

Assumption 3. *The time derivatives of the control inputs (i.e., $\dot{\beta}$ and $\dot{\tau}_g$) are bounded over the operating domain $\mathcal{O}$. The function $\mathcal{F}(\cdot)$, which involves $\dot{v}$ and $\dot{\delta}(t)$, is unknown but is assumed to be bounded over $\mathcal{O}$.* ■

Given that the function $\mathcal{F}(\cdot)$ is not well-known, it can not appear in the observer. A solution for the observation of the system defined by Eq. (19) is a robust one proposed by (Levant, 2003). Thus, consider the canonical form Eq. (19) that is a perturbed uncertain double integrator. From (Levant, 2003), the supertwisting-based observer reading as

$$\begin{aligned} \dot{\hat{z}}_1 &= \hat{z}_2 + \underbrace{L_{\phi_1}^{1/2} a_1 \left|z_1 - \hat{z}_1\right|^{1/2} \mathrm{sign}(z_1 - \hat{z}_1)}_{\gamma_1(z_1,\hat{z}_1)} \\ \dot{\hat{z}}_2 &= \underbrace{L_{\phi_1} a_2 \,\mathrm{sign}(z_1 - \hat{z}_1)}_{\gamma_2(z_1,\hat{z}_1)} \end{aligned} \tag{21}$$

with a_1 and a_2 constant values fixed as suggested in (Levant, 2003), $a_1 = 1.5$ and $a_2 = 1.1$ and

$$L_{\phi_1} > \left|\mathcal{F}(z_1, z_2, \beta, \dot{\beta}, \tau_g, \dot{\tau}_g, t)\right| \tag{22}$$

ensures $\hat{z} = [\hat{z}_1\ \hat{z}_2]^\top \to [z_1\ z_2]^\top$ in a finite time in spite of the perturbations and uncertainties.

Theorem 1. *Consider the system in Eq.* (8) *and Assumptions 1-4 fulfilled. Suppose that it is locally observable in the sense of Definition 1. So, the system (with Φ defined by Eq.* (16)*)*

$$\dot{\hat{x}} = \begin{bmatrix} \dot{\hat{\omega}} \\ \dot{\hat{v}} \end{bmatrix} = F(\hat{x}, u) + \left[\frac{\partial \Phi}{\partial \hat{x}}\right]^{-1} \cdot \begin{bmatrix} L_{\phi_1}^{1/2} a_1 |\omega - \hat{\omega}|^{1/2} \,\mathrm{sign}(\omega - \hat{\omega}) \\ L_{\phi_1} a_2 \,\mathrm{sign}(\omega - \hat{\omega}) \end{bmatrix} \tag{23}$$

is an observer of Eqs. (7)-(8) *with a_1 and a_2 constant values fixed as suggested in (Levant, 2003), $a_1 = 1.5$ and $a_2 = 1.1$, and the constant L_{ϕ_1} such that*

$$L_{\phi_1} > \left|\frac{\mathrm{d}}{\mathrm{d}t}\left[\frac{\rho\pi R^3 v^2}{2J\lambda} C_p(\lambda,\beta)\right] - \frac{n_g}{J}\dot{\tau}_g + \dot{\delta}(t)\right| \tag{24}$$

■

Proof of Theorem 1. The observer represented by Eq. (21) has been designed based on the nominal system of Eq. (19) without the uncertain/perturbed term $\mathcal{F}(\cdot)$ in its definition; the gain tuning is based on the bound of $\mathcal{F}(\cdot)$. By a similar way, the writing

https://doi.org/10.5194/wes-2025-206
Preprint. Discussion started: 21 November 2025
© Author(s) 2025. CC BY 4.0 License.

of the observer in Eq. (21) in the $\hat{x}$-state space, that is Eq. (23) is based on the state coordinate transformation $\hat{z} = \Phi(\hat{x}, u)$, but without taking into account perturbations and uncertainties. Firstly, consider

$$z = \Phi(x, u) \tag{25}$$

that gives

$$\dot{z} = \frac{\partial \Phi}{\partial x}\dot{x} + \frac{\partial \Phi}{\partial u}\dot{u} \tag{26}$$

Then, by considering no perturbation or uncertainties, one gets

$$F(x, u) = \left[\frac{\partial \Phi}{\partial x}\right]^{-1}\left(Az - \frac{\partial \Phi}{\partial u}\dot{u}\right) \tag{27}$$

with

$$A = \begin{bmatrix} 0 & 1 \\ 0 & 0 \end{bmatrix}$$

Design now the observer of Eq. (21) in the $\hat{x}$-state space starting from the state coordinate transformation

$$\hat{z} = \Phi(\hat{x}, u) \tag{28}$$

by considering no uncertainties and perturbation (given that here is considered the observer design—perturbation and uncertainties are managed by the correction terms of the observer). One gets

$$\begin{aligned} \dot{\hat{x}} &= \left[\frac{\partial \Phi}{\partial \hat{x}}\right]^{-1} \cdot \left(\dot{\hat{z}} - \frac{\partial \Phi}{\partial u}\dot{u}\right) \\ &= \left[\frac{\partial \Phi}{\partial \hat{x}}\right]^{-1} \cdot \left(A\hat{z} + \begin{bmatrix} \gamma_1(\cdot) \\ \gamma_2(\cdot) \end{bmatrix} - \frac{\partial \Phi}{\partial u}\dot{u}\right) \\ &= \underbrace{\left[\frac{\partial \Phi}{\partial \hat{x}}\right]^{-1} \cdot \left(A\hat{z} - \frac{\partial \Phi}{\partial u}\dot{u}\right)}_{F(\hat{x}, u) \text{ from Eq. (27)}} + \left[\frac{\partial \Phi}{\partial \hat{x}}\right]^{-1} \cdot \begin{bmatrix} \gamma_1(\cdot) \\ \gamma_2(\cdot) \end{bmatrix} \end{aligned} \tag{29}$$

that is the form of system displayed in Theorem 1. Given that system in Eq. (21) is an observer for Eq. (19) under condition Eq. (22), then system in Eq. (29) is an observer for Eq. (8) if condition Eq. (24) is fulfilled with $a_1 = 1.5$ and $a_2 = 1.1$. ■

3.3 Adaptive observer gain

A drawback of the proposed approach is that the term L_{ϕ_1} is difficult to carefully tune, because determining the bound of

$$\left|\frac{\mathrm{d}}{\mathrm{d}t}\left[\frac{\rho\pi R^3 v^2}{2J\lambda}C_p(\lambda, \beta)\right] - \frac{n_g}{J}\dot{\tau}_g + \dot{\delta}(t)\right| \tag{30}$$

is a very hard task that could give an overestimation and then induce chattering phenomenon. A solution consists in using an adaptive version of the supertwisting-based observer (Mirzaei et al., 2022) allowing to have an online tuning of the observer, thanks to the evaluation on only the estimation error of ω. The principle is the following

https://doi.org/10.5194/wes-2025-206
Preprint. Discussion started: 21 November 2025
© Author(s) 2025. CC BY 4.0 License.

eawe european academy of wind energy
Open Access WIND ENERGY SCIENCE DISCUSSIONS

– if the estimation error of ω is large, it could be due to too small gains versus the uncertainties/perturbations effects. Then, gain adaptation law is defined in order to increase the gains of the observers;

– in the opposite case, *i.e.* if the estimation error of ω is small, it means that the observer gains are enough large. Then, gain adaptation law is defined in order to reduce them.

So, the observer in Eq. (23) is replaced by its adaptive version reading as (Mirzaei et al., 2022)

$$\dot{\hat{x}} = \begin{bmatrix} \dot{\hat{\omega}} \\ \dot{\hat{v}} \end{bmatrix} = F(\hat{x}, u) + \left[\frac{\partial \Phi}{\partial \hat{x}}\right]^{-1} \cdot \begin{bmatrix} k_1 \, |\omega - \hat{\omega}|^{1/2} \, \mathrm{sign}(\omega - \hat{\omega}) \\ k_2 \, \mathrm{sign}(\omega - \hat{\omega}) \end{bmatrix} \tag{31}$$

with

$$\begin{aligned} \dot{k}_1 &= \begin{cases} \dfrac{\alpha}{|\psi| + \varepsilon}, & \text{if } |\omega - \hat{\omega}| > \varepsilon, \\ -k_1, & \text{if } |\omega - \hat{\omega}| \leq \varepsilon \end{cases}, \quad k_1(0) > 0 \\ \dot{k}_2 &= \begin{cases} \dfrac{\alpha}{2\,|\omega - \hat{\omega}|^{1/2}}, & \text{if } |\omega - \hat{\omega}| > \varepsilon, \\ -k_2, & \text{if } |\omega - \hat{\omega}| \leq \varepsilon \end{cases}, \quad k_2(0) > 0 \end{aligned} \tag{32}$$

with $\psi = \dfrac{\mathrm{d}}{\mathrm{d}t}(\omega - \hat{\omega})$.

In Fig. 2, the overall estimation framework is illustrated. The rotor speed ω is the only measured signal, whereas the generator torque τ_g and the blade pitch angle β serve as known control inputs. These quantities are used within a reduced-order, observation-oriented model (Sect. 2), upon which three estimators are implemented: the SOSMO, its adaptive version ASOSMO, and the CD-EKF. Each estimator provides estimates of both the wind speed $\hat{v}$ and the rotor speed $\hat{\omega}$. The CD-EKF serves as a benchmark for assessing the performance of the proposed sliding-mode estimators.

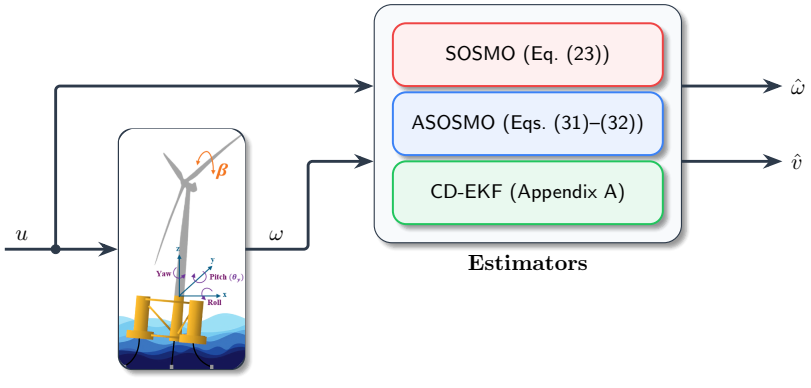

Figure 2. Overview of the estimator architecture proposed in this work, in which the rotor speed ω is the only measured signal. The outputs $\hat{v}$ and $\hat{\omega}$ denote the estimated wind and rotor speeds, respectively.

https://doi.org/10.5194/wes-2025-206
Preprint. Discussion started: 21 November 2025
© Author(s) 2025. CC BY 4.0 License.

eawe european academy of wind energy
Open Access WIND ENERGY SCIENCE DISCUSSIONS

4 Simulation results

In this section, the performances of the proposed wind speed observers are evaluated and compared with the CD-EKF used in ROSCO, which is described in A. All simulations are conducted on the NREL 5 MW FOWT, supported by a semi-submersible platform. The simulation environment integrates MATLAB/SIMULINK 2023a for implementing the observers and control algorithms with OpenFAST (Jonkman et al., 2009), which simulates the high-fidelity aero-hydro-servo-elastic model of the FOWT. Each test is run for 800 seconds under identical wind and wave conditions, with a fixed sampling time of 0.0125 seconds.

Although the observer design is based on the reduced-order model in Eq. (5), all 24 degrees of freedom available in OpenFAST are activated in the simulations to ensure a comprehensive evaluation under realistic conditions.

First, a realistic turbulent wind profile is considered, and the experimental results for three cases are presented in Section 5.

4.1 Turbulent wind scenario

Realistic turbulent wind profiles are generated using TurbSim (Jonkman, 2009), with a mean wind speed of 18 m s^{-1}, following the widely adopted Kaimal turbulence model. Additionally, irregular wave conditions are modeled using the HydroDyn module (Jonkman et al., 2014) within OpenFAST, with a significant wave height of 3.25 m. Both environmental conditions are illustrated in Fig. 3.

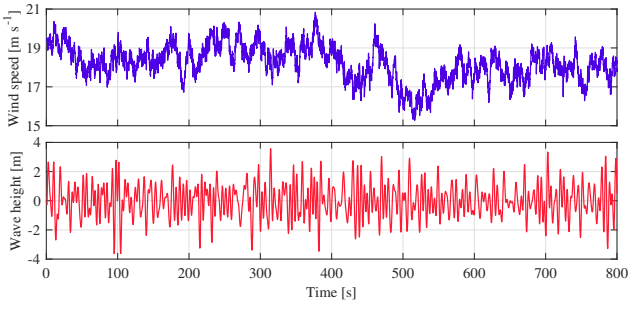

Figure 3. Environmental conditions used in the simulations: turbulent wind speed (top) generated by TurbSim, and irregular wave elevation (bottom) generated by the HydroDyn module.

In the first case, the following observers are compared: SOSMO based on supertwisting in Eq. (23), its adaptive version in Eqs. (31)–(32), and CD-EKF used in the ROSCO.

Prior to evaluating their performances, the system's observability is verified from Eq. (15). Figure 4 illustrates the evolution of the Eq. (15). Its consistently nonzero behavior confirms that Φ is invertible, thereby ensuring observability of the nonlinear system under stochastic wind conditions.

With the observability condition satisfied in Fig. 4, the estimation performance of the three observers in Fig. 2 is subsequently assessed.

https://doi.org/10.5194/wes-2025-206
Preprint. Discussion started: 21 November 2025
© Author(s) 2025. CC BY 4.0 License.

eawe european academy of wind energy
Open Access WIND ENERGY SCIENCE DISCUSSIONS

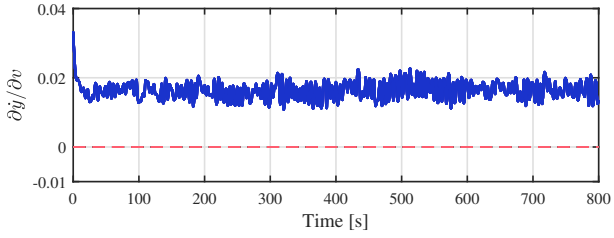

Figure 4. Time evolution of the observability condition given in Eq. (15).

4.1.1 Second-order sliding mode observer (SOSMO)

Figure 5 shows the rotor speed and wind speed estimation results for the SOSMO. Despite its relatively simple structure, the SOSMO achieves acceptable estimation performance. A notable property in Fig. 5 is the filtering effect of the SOSMO compared with the measured wind speed.

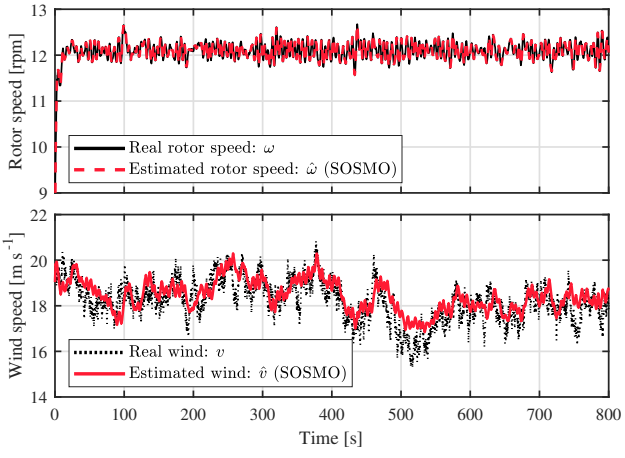

Figure 5. Rotor speed (above) and wind speed (bottom) estimation results of SOSMO defined in Eq. (23).

4.1.2 Adaptive second-order sliding mode observer (ASOSMO)

Figure 6 presents the rotor speed and wind speed estimation results of the ASOSMO. The distinguishing feature of ASOSMO is its ability to adapt observer gains online, which enhances robustness against model uncertainties and time-varying operating conditions. Unlike the previous SOSMO that relies on fixed gains, ASOSMO continuously adjusts its gains based on real-time system behavior, reducing the dependence on accurate prior model knowledge. As illustrated in Fig. 7, the adaptive gains evolve dynamically during the estimation process, responding effectively to state variations.

https://doi.org/10.5194/wes-2025-206
Preprint. Discussion started: 21 November 2025
© Author(s) 2025. CC BY 4.0 License.

eawe european academy of wind energy
Open Access WIND ENERGY SCIENCE DISCUSSIONS

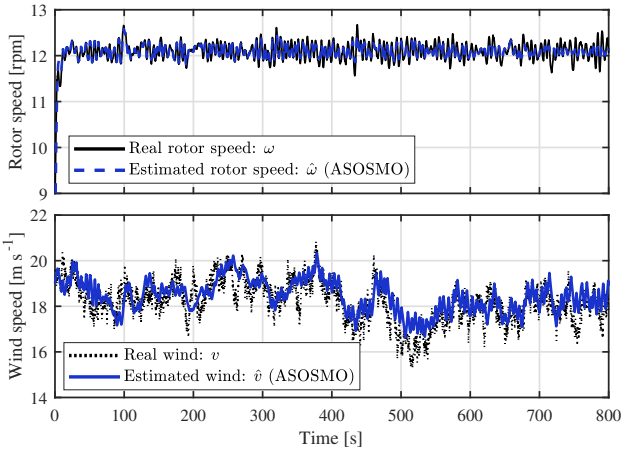

Figure 6. Rotor speed (above) and wind speed (bottom) estimation results of ASOSMO defined in Eqs. (31)–(32).

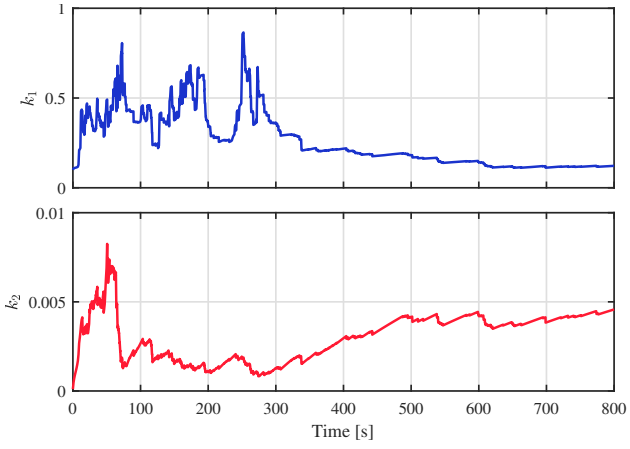

Figure 7. Evolution of adaptation gains k_1 (top) and k_2 (bottom) in the ASOSMO Eqs. (31)–(32).

4.1.3 Continuous-discrete extended Kalman filter (CD-EKF)

Figure 8 shows the results for the CD-EKF used in ROSCO. This method achieves smooth and accurate estimates. However, its implementation is more complex, requiring careful tuning of covariance matrices and linearization of system dynamics, which can be computationally demanding and sensitive to modeling errors.

A comparative evaluation of all three observers is presented in Table 1. The table reports the wind speed estimation accuracy of the three observers under a turbulent wind scenario. The performance metric used is the root mean square error of the estimation error (*i.e.*, $v - \hat{v}$). The both sliding mode-based estimators demonstrate improved precision, with RMSE values of 0.66 and 0.67, respectively, in contrast to the CD-EKF method, which has an RMSE of 0.77. The SOSMO method demonstrates a relative reduction of approximately $14\ \%$ in wind speed RMSE when compared with CD-EKF, whereas ASOSMO exhibits

https://doi.org/10.5194/wes-2025-206
Preprint. Discussion started: 21 November 2025
© Author(s) 2025. CC BY 4.0 License.

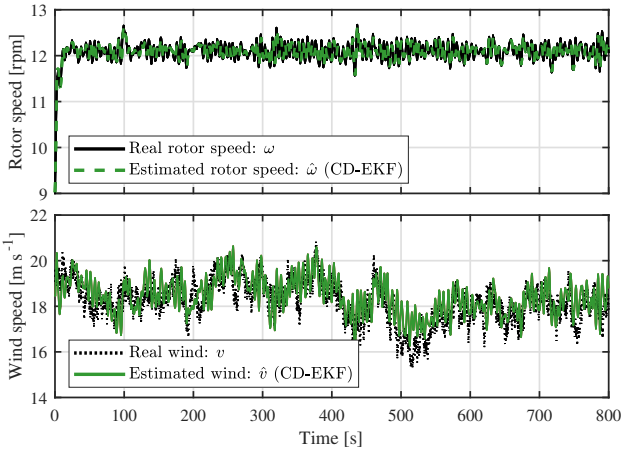

Figure 8. Rotor speed (above) and wind speed (bottom) estimation results of CD-EKF.

a reduction of about 13 %. The findings demonstrate the efficacy of sliding mode-based observers in enhancing estimation accuracy while preserving a lower computational cost.

Table 1. Comparison of wind speed root mean square estimation error (RMSE) for different estimators.

Estimator	RMSE of wind speed estimation
SOSMO	0.66
ASOSMO	0.67
CD-EKF	0.77

Note. Lower values indicate better estimation performance.

Overall, while all three observers are capable of delivering reliable estimations, the SOSMO offers a balance between simplicity and performance. ASOSMO introduces adaptive capability with limited system knowledge, and CD-EKF, though robust, involves a more complex design process. In this context, both the constant-gain and adaptive versions of the SOSMO are considered practical and effective solutions for wind turbine state estimation under varying wind scenarios.

4.2 Computational time

To assess the computational burden of each observer, execution times were measured in MATLAB 2023a simulations under identical conditions (Sect. 4.1). The CD-EKF exhibited the longest runtime (18 ms), followed by the ASOSMO (11 ms) and the SOSMO (9 ms). These results reflect the higher algorithmic complexity of the CD-EKF, as expected. The ASOSMO slightly increases complexity with its adaptive gain mechanism, in contrast to the constant gain used in the SOSMO (see Fig. 9).

https://doi.org/10.5194/wes-2025-206
Preprint. Discussion started: 21 November 2025
© Author(s) 2025. CC BY 4.0 License.

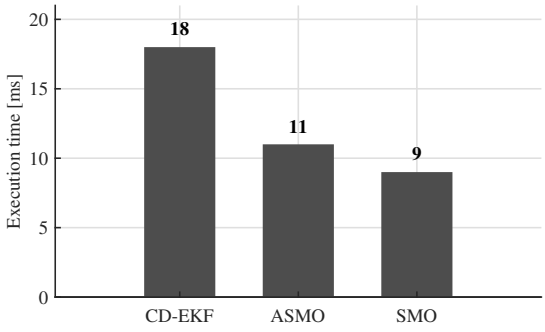

Figure 9. Execution time (in milliseconds) of different observers measured in MATLAB simulations under identical conditions.

5 Experimental results

The proposed observers have been experimentally validated on a SIL setup at École Centrale Nantes, France. The experimental platform consists of a 1/32-scale semisubmersible FOWT, based on the OC4-DeepCwind concept, deployed in the wave tank of the LHEEA Laboratory (LHEEA Laboratory, 2025).

As shown in Fig. 10, aerodynamic loads are emulated in real time by a six-fan thrust generator mounted on the turbine's tower, driven by aerodynamic inputs from the OpenFAST simulation. Simultaneously, wave generators in the tank reproduce hydrodynamic conditions, ensuring realistic environmental forcing. A six degrees of freedom actuation system replaces the drive-train, enabling closed-loop testing under dynamic conditions (Ferahtia et al., 2025).

Table 2 outlines selected technical characteristics of both the numerical emulator (OpenFAST) and the scaled experimental setup implemented in the laboratory. The table highlights key parameters of the reference full-scale FOWT alongside those used in the physical test environment.

5.1 Test conditions and scenarios

Three test scenarios have been conducted to evaluate the performance and robustness of the proposed observers under various wind and wave conditions, as reported in Table 3. The three datasets were selected under complementary operating regimes as

- **Case 1 (Region III only).** With $v \in [11.41, 25.37]$ m s^{-1}, the turbine operates fully above rated only, highlighting estimator behavior under above-rated operation and strong pitch activity.
- **Case 2 (Transition Region II↔III).** With $v \in [8.20, 14.42]$ m s^{-1}, it covers the transition region, testing robustness to region switching.
- **Case 3 (Region II/III).** With $v \in [8.43, 19.24]$ m s^{-1}, serving as a general verification across variable conditions from low wind speed to high wind speed.

https://doi.org/10.5194/wes-2025-206
Preprint. Discussion started: 21 November 2025
© Author(s) 2025. CC BY 4.0 License.

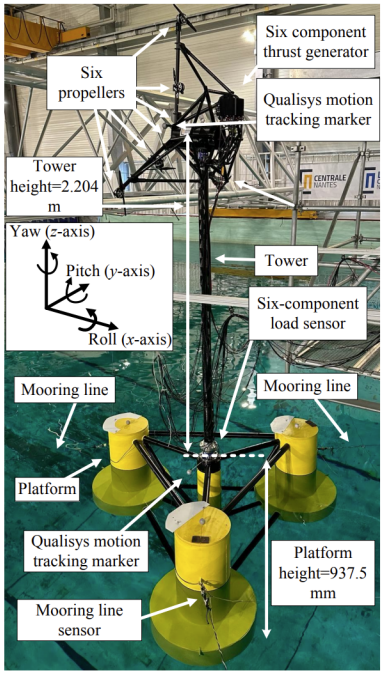

Figure 10. Experimental SIL test setup of the 5 MW 1/32-scale semisubmersible OC4 FOWT at *École Centrale Nantes* (Aslmostafa et al., 2024).

Table 2. Key specifications of the experimental setup, including both full-scale and corresponding 1/32-scale parameters.

Parameter	Real : model scale	Unit
Floater type	Semi-submersible[a]	–
Nominal power[b]	5	MW
Rotor diameter[b]	126	m
Platform height	30 : 0.9375	m
Tower height	70.528 : 2.204	m
Tower mass	2.5×10^5 : 8	kg
Rotor thrust	8.0×10^5 : 24.4	N
Test tank size	$50 \times 30 \times 5$	m

Notes. [a] Based on the OC4-DeepCwind platform under IEA Wind Task 30 (Robertson et al., 2014)
[b] Emulated via software-in-the-loop (SIL).

The three cases collectively address various conditions to ensure a balanced comparison of CD-EKF, SOSMO, and ASOSMO against the actual wind speed.

https://doi.org/10.5194/wes-2025-206
Preprint. Discussion started: 21 November 2025
© Author(s) 2025. CC BY 4.0 License.

eawe european academy of wind energy
Open Access WIND ENERGY SCIENCE DISCUSSIONS

Table 3. Test conditions for experimental validation, including wind and wave ranges and region classification based on turbine operating regimes.

	Wind speed ($\mathrm{m\,s^{-1}}$)		Wave elevation (m)		Region[a]	
Test case	Min	Max	Min	Max	II	III
Case 1	11.41	25.37	−4.62	5.54	–	✓
Case 2	8.20	14.42	−2.48	2.89	✓	✓
Case 3	8.43	19.24	−2.35	2.92	✓	✓

Note. [a] Region II: $3 \leq v < 11.4\ \mathrm{m\,s^{-1}}$; Region III: $11.4 \leq v \leq 25\ \mathrm{m\,s^{-1}}$ (Jonkman et al., 2009).

5.2 Results and discussion

Figures 11–13 illustrate the experimental results for the three test cases. In all scenarios, observers are able to estimate the wind speed despite the presence of wave-induced platform motions and unmodeled dynamics.

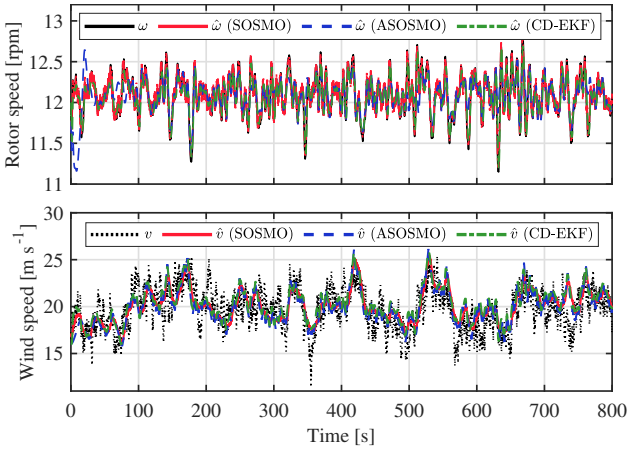

Figure 11. Experimental results for case 1: rotor speed ω, wind speed v, and their estimated values under turbulent wind and wave conditions.

Evaluation of root mean square of estimation error $v - \hat{v}$ is reported in Table 4. In all three test cases, both sliding mode observers outperformed the CD-EKF. Specifically, SOSMO achieves RMSE reductions of 6.4 %, 18.5 %, and 13.6 % in Cases 1 through 3, respectively, compared with CD-EKF. The adaptive version (ASOSMO) also demonstrates improvements in cases 1, 2 and 3, with RMSE reductions of 1.64 %, 15.7 % and 10.6 %, respectively.

To facilitate comparison across the three cases, Fig. 14 presents the normalized RMSE values for each observer, with normalization performed with respect to CD-EKF.

https://doi.org/10.5194/wes-2025-206
Preprint. Discussion started: 21 November 2025
© Author(s) 2025. CC BY 4.0 License.

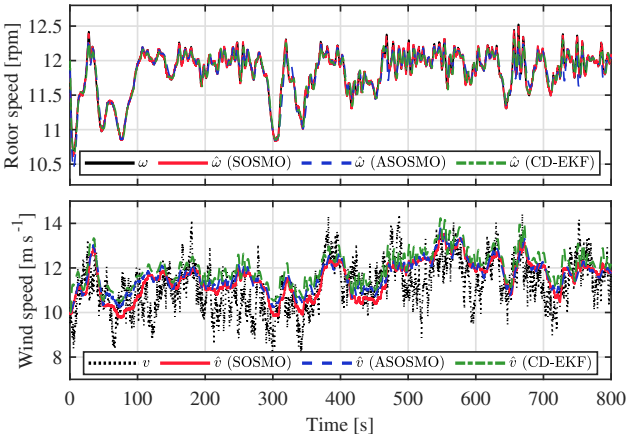

Figure 12. Experimental results for case 2: rotor speed ω, wind speed v, and their estimated values under turbulent wind and wave conditions.

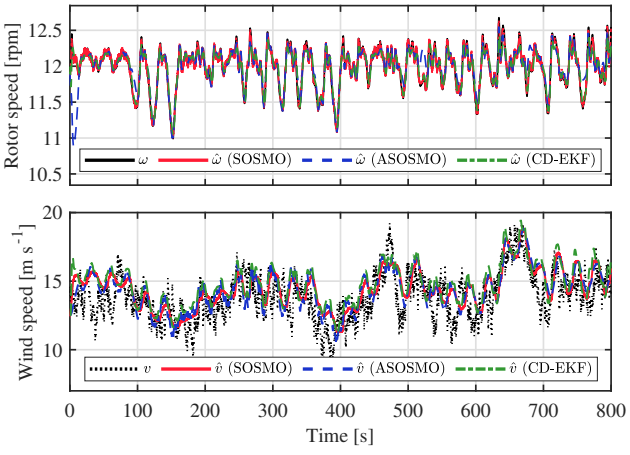

Figure 13. Experimental results for case 3: rotor speed ω, wind speed v, and their estimated values under turbulent wind and wave conditions.

Table 4. Evaluation of observer performance based on root mean square of $v-\hat{v}$ of wind speed estimates in dynamic experimental conditions.

Method	Case 1	Case 2	Case 3
CD-EKF	1.88	1.21	1.72
SOSMO	1.76	0.99	1.48
ASOSMO	1.85	1.02	1.54

Note. RMSE computed on $v-\hat{v}$; lower is better.

Overall, the experimental findings align well with the simulation results. The proposed SOSMOs exhibit robustness, low computational cost, and reduced tuning complexity, combined with estimation accuracy, that make SOSMO and ASOSMO attractive for practical deployment in FOWT control frameworks.

https://doi.org/10.5194/wes-2025-206
Preprint. Discussion started: 21 November 2025
© Author(s) 2025. CC BY 4.0 License.

eawe european academy of wind energy
Open Access WIND ENERGY SCIENCE DISCUSSIONS

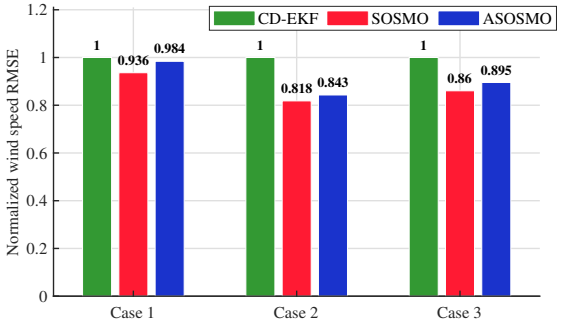

Figure 14. Normalized wind speed RMSE comparison across three estimators (CD-EKF, SOSMO, and ASOSMO) for the three experimental test cases. Each bar represents the RMSE normalized *w.r.t.* the CD-EKF solution.

6 Conclusions

This paper proposed robust wind speed estimation methods based on a second-order sliding mode observer: a constant-gain second-order sliding mode observer (SOSMO) and its adaptive version (ASOSMO). The estimation framework is built on a reduced-order nonlinear model and is validated not only on the OpenFAST simulator but also through experimental tests where all degrees of freedom are activated.

The two observers are evaluated against the standard continuous–discrete extended Kalman filter (CD-EKF), and they demonstrate accurate tracking of wind dynamics. Unlike CD-EKF, the SOSMO-based methods not only eliminate the need for tuning noise covariance matrices but also avoid the linearization of system dynamics, thereby reducing implementation complexity and improving reliability under modeling uncertainties. Moreover, the adaptive version allows for very limited knowledge of the model.

To summarize, the proposed observers provide a simple yet effective solution for accurate wind speed estimation and can be integrated into advanced control strategies. This integration promises improved system stability and reduced fatigue loads, contributing significantly to the performance of FOWTs. These results mark an initial step toward a comprehensive robust estimation and control framework.

As future work, a fully integrated adaptive observer/controller scheme will be developed to further improve the overall performance and resilience of FOWTs.

Appendix A: Continuous-discrete extended Kalman filter

The nonlinear state-space form of a FOWT can be written as:

$$\begin{aligned} \dot{x} &= f(x,u) + w(t), \\ y_k &= h(x_k,u_k) + v_k(t_k), \end{aligned} \tag{A1}$$

https://doi.org/10.5194/wes-2025-206
Preprint. Discussion started: 21 November 2025
© Author(s) 2025. CC BY 4.0 License.

eawe european academy of wind energy
Open Access WIND ENERGY SCIENCE DISCUSSIONS

where $\mathbf{x} = \begin{bmatrix} \omega_r & v_t & v_m \end{bmatrix}^\top$ is the state-space vector, v_t and v_m denote the turbulent and mean components of the wind speed, respectively, and the control input is $u = \beta$. Additionally $w(t)$ and v_k are continuous white noise and discrete-time white noise, respectively, which are defined as

$$w(t) \sim \mathcal{N}(0, Q),$$
$$v_k \sim \mathcal{N}(0, R_k), \tag{A2}$$

where Q is the process noise covariance matrix and R_k is the measurement noise covariance matrix.

The extended Kalman filter for a continuous–discrete nonlinear system generally consists of two main steps: (i) time update (prediction) and (ii) measurement update (correction), as described in (Abbas et al., 2022; Knudsen et al., 2011) as

• Step 1: Time update

$$\hat{x}_0^+ = \mathbb{E}(x_0), \tag{A3}$$
$$\hat{P}_0^+ = \mathbb{E}\left[(x_0 - \hat{x}_0)(x_0 - \hat{x}_0)^\top\right], \tag{A4}$$
$$\dot{\hat{x}}(t) = f(\hat{x}_{k-1|k-1}, u_k), \tag{A5}$$
$$\dot{P}(t) = F(t)P_{k|k} + P_{k|k}F^\top(t) + Q_k - K_{k-1}R_m K_{k-1}^\top, \tag{A6}$$

where $F(t) = \frac{\partial f}{\partial \mathbf{x}}\Big|_{\hat{\mathbf{x}}_{k-1|k-1}, u_k}$ is the Jacobian matrix $f(x, u)$. additionally $\hat{P}$ is the estimation error covariance. In the above equations, the term $\hat{x}^+$ represents the estimate of x_k using the information from y_k, while $\hat{x}^-$ denotes the estimate of x_k using the measurement from y_{k-1}.

• Step2: Measurement update

$$K_k = P_{k|k-1}H_k^\top \left(H_k P_{k|k-1} H_k^\top + R_m\right)^{-1}, \tag{A7}$$
$$\hat{\mathbf{x}}_{k|k} = \hat{\mathbf{x}}_{k|k-1} + K_k(y_k - h(\hat{x}_{k|k-1})), \tag{A8}$$
$$P_{k|k} = (I - K_k H_k)P_{k|k-1}, \tag{A9}$$

where $H_k = \frac{\partial h}{\partial \mathbf{x}}\Big|_{\hat{\mathbf{x}}_{k|k-1}}$ is the Jacobian matrix of $h(\mathbf{x}_k)$, and K_k is the Kalman gain. By defining

$$Q = \mathrm{diag}\left\{1 \times 10^{-5},\ \frac{\pi v_m^3 t_i^2}{L},\ \frac{4}{600}\right\}, \quad R_m = 0.02, \tag{A10}$$

and using the relation $\hat{v} = v_t + v_m$, the estimation of the wind speed is calculated.

https://doi.org/10.5194/wes-2025-206
Preprint. Discussion started: 21 November 2025
© Author(s) 2025. CC BY 4.0 License.

eawe european academy of wind energy
Open Access WIND ENERGY SCIENCE DISCUSSIONS

Appendix B: Nomenclature

Abbreviations

ASOSMO	Adaptive second-order sliding mode observer
CD-EKF	Continuous–discrete extended Kalman filter
EKF	Extended Kalman filter
FOWT	Floating offshore wind turbine
KF	Kalman filter
NREL	National Renewable Energy Laboratory
RMSE	Root mean square error
ROSCO	Reference open-source controller
SIL	Software-in-the-loop
SMO	Sliding mode observer
SOSMO	Second-order sliding mode observer
STW	Supertwisting

Symbols and parameters

α, ε	Design parameters of the adaptive law [–]
β	Blade pitch angle [rad]
λ	Tip-speed ratio [–]
ω, $\hat{\omega}$	Real and estimated rotor speed [rad s^{-1}]
ρ	Air density [kg m^{-3}]
τ_a	Aerodynamic torque [N m]
τ_g, τ_g^*	Generator torque, rated value [N m]
C_p	Power coefficient (function of λ, β) [–]
J	Total rotational inertia [kg m^2]
k_1, k_2	Adaptive observer gains [–]
n_g	Gearbox ratio [–]
P_a	Aerodynamic power extracted by the rotor [W]
P_{wind}	Theoretical wind power [W]
R	Rotor radius [m]
u	Control input vector
v, $\hat{v}$	True and estimated wind speed [m s^{-1}]
z	Observer coordinate vector

https://doi.org/10.5194/wes-2025-206
Preprint. Discussion started: 21 November 2025
© Author(s) 2025. CC BY 4.0 License.

eawe european academy of wind energy
Open Access WIND ENERGY SCIENCE DISCUSSIONS

Author contributions. **Moein Sarbandi**: Writing – original draft, supervision, validation. **Matis Viozelange**: Methodology, writing. **Mohamed Assaad Hamida**: Methodology, conceptualization. **Franck Plestan**: Conceptualization, writing – review and editing, supervision, project administration.

Competing interests. The contact author has declared that neither he nor any of the co-authors have any competing interests.

Acknowledgements. This project has received funding from European Union's Framework Programme for Research and Innovation Europe Horizon Europe (HORIZON) Marie Skłodowska-Curie Actions Doctoral Networks (MSCA-DN) under the Grant Agreement No. 101120278 - DENSE. The authors also thank the experimental team and researchers at LHEEA / École Centrale Nantes – CNRS, who contributed to the experimental campaign and corresponding database developed within the ANR project CREATIF (ANR-20-CE05-0039), France. During the preparation of this manuscript, AI tools (specifically ChatGPT) were used solely for grammatical correction and to improve readability. The authors conducted multiple rounds of revision independently. At no stage were these tools employed to generate, modify, or verify any scientific results or methodological approaches. All scientific ideas and methodologies were developed entirely by the authors.

https://doi.org/10.5194/wes-2025-206
Preprint. Discussion started: 21 November 2025
© Author(s) 2025. CC BY 4.0 License.

eawe european academy of wind energy
Open Access WIND ENERGY SCIENCE DISCUSSIONS

References

Abbas, N. J., Zalkind, D. S., Pao, L., and Wright, A.: A reference open-source controller for fixed and floating offshore wind turbines, Wind Energy Science, 7, 53–73, 2022.

Aslmostafa, E., Mirzaei, M., Mojallizadeh, M., Hamida, M., and Plestan, F.: Robust control strategies for floating wind turbines: preliminary experimental results, in: 2024 17th International Workshop on Variable Structure Systems (VSS), pp. 298–303, IEEE, Abu Dhabi, United Arab Emirates, 2024.

Aslmostafa, E., Hamida, M., Shtessel, Y., Laghrouche, S., and Plestan, F.: A unified controller for a floating wind turbine evolving in Region II and Region III: preliminary experimental results, in: 2025 American Control Conference (ACC), pp. 1494–1499, Denver, CO, USA, 2025.

Barambones, O., Cortajarena, J. A., Calvo, I., Gonzalez de Durana, J. M., Alkorta, P., and Karami-Mollaee, A.: Real time observer and control scheme for a wind turbine system based on a high order sliding modes, Journal of the Franklin Institute, 358, 5795–5819, 2021.

Boukhezzar, B. and Siguerdidjane, H.: Nonlinear Control of a Variable-Speed Wind Turbine Using a Two-Mass Model, IEEE Transactions on Energy Conversion, 26, 149–162, 2011.

Castillo, O. C., Andrade, V. R., Rivas, J. J. R., and González, R. O.: Comparison of Power Coefficients in Wind Turbines Considering the Tip Speed Ratio and Blade Pitch Angle, Energies, 16, 2023.

Chen, H., Niu, J., Cai, Y., Aït-Ahmed, N., Aït-Ahmed, M., and Benbouzid, M.: Adaptive sliding mode-based feedback linearization control for floating offshore wind turbine in region II, International Journal of Green Energy, 22, 467–486, 2025.

Chen, P. and Han, D.: Effective wind speed estimation study of the wind turbine based on deep learning, Energy, 247, 123 491, 2022.

Davila, J., Fridman, L., and Levant, A.: Second-order sliding-mode observer for mechanical systems, IEEE Transactions on Automatic Control, 50, 1785–1789, https://doi.org/10.1109/TAC.2005.858636, 2005.

Ferahtia, S., Houari, A., Machmoum, M., Mojallizadeh, M. R., Ait-Ahmed, M., and Bonnefoy, F.: Floating Offshore Wind Turbine Optimized Control for Power Regulation With Experimental Validation, IEEE Journal of Oceanic Engineering, 50, 1231–1243, 2025.

Global Wind Energy Council: Floating offshore wind – A global opportunity, 2022.

Gräfe, M., Pettas, V., Gottschall, J., and Cheng, P. W.: Quantification and correction of motion influence for nacelle-based lidar systems on floating wind turbines, Wind Energy Science, 8, 925–946, 2023.

He, S., Wang, B., and Chen, Y.: Improved optimal torque control for large scale floating offshore wind turbines based on interval type-2 fuzzy logic system, Ocean Engineering, 330, 121 186, 2025.

Hernández, J., Guadayol, M., and Puig, V.: Wind speed estimation in wind turbines using EKF: Application to experimental data, in: 2014 UKACC International Conference on Control, pp. 474–479, IEEE, Loughborough, UK, 2014.

Jena, D. and Rajendran, S.: A review of estimation of effective wind speed based control of wind turbines, Renewable and Sustainable Energy Reviews, 43, 1046–1062, 2015.

Jonkman, B. J.: TurbSim user's guide: Version 1.50, Tech. rep., National Renewable Energy Laboratory, Golden, CO (United States), 2009.

Jonkman, J., Butterfield, S., Musial, W., and Scott, G.: Definition of a 5-MW Reference Wind Turbine for Offshore System Development, National Renewable Energy Laboratory, 2009.

Jonkman, J. M., Robertson, A. N., and Hayman, G. J.: HydroDyn User's Guide and Theory Manual, Tech. rep., National Renewable Energy Laboratory, Golden, CO (United States), 2014.

https://doi.org/10.5194/wes-2025-206
Preprint. Discussion started: 21 November 2025
© Author(s) 2025. CC BY 4.0 License.

Kim, D., Jeon, T., Paek, I., and Roynarin, W.: Comparison of the Wind Speed Estimation Algorithms of Wind Turbines Using a Drive Train Model and Extended Kalman Filter, Applied Sciences, 14, 8764, 2024.

Knudsen, T., Bak, T., and Soltani, M.: Prediction models for wind speed at turbine locations in a wind farm, Wind Energy, 14, 877–894, 2011.

Krener, A. and Respondek, W.: Nonlinear observers with linearizable error dynamics, SIAM J. Control Optim., 23, 197–216, 1985.

Levant, A.: Sliding order and sliding accuracy in sliding mode control, International Journal of Control, 58, 1247–1263, 1993.

Levant, A.: High-order sliding modes: differentiation and output-feedback, Int. J. Control, 76, 924–941, 2003.

LHEEA Laboratory: LHEEA Laboratory - École Centrale de Nantes, https://lheea.ec-nantes.fr/, 2025.

Li, J. and Geng, H.: Platform Pitch Motion Suppression for Floating Offshore Wind Turbine in Above-Rated Wind Speed Region, IEEE Transactions on Sustainable Energy, 15, 1994–2005, 2024.

Ma, R., Siaw, F. L., Thio, T. H. G., and Yang, W.: New adaptive super-twisting extended-state observer-based sliding mode scheme with application to fowt pitch control, Journal of Marine Science and Engineering, 12, 902, 2024.

Mahdizadeh, A., Schmid, R., and Oetomo, D.: LIDAR-Assisted Exact Output Regulation for Load Mitigation in Wind Turbines, IEEE Transactions on Control Systems Technology, 29, 1102–1116, 2021.

Manwell, J. F., McGowan, J. G., and Rogers, A. L.: Wind energy explained: Theory, design and Application, Wiley, Chichester, U.K., 2009.

McCoy, A., Musial, W., Hammond, R., Mulas Hernando, D., Duffy, P., Beiter, P., Perez, P., Baranowski, R., Reber, G., and Spitsen, P.: Offshore Wind Market Report: 2024 Edition, Tech. rep., National Renewable Energy Laboratory (NREL), Golden, CO (United States), 2024.

Mirzaei, M. J., Hamida, M. A., Plestan, F., and Taleb, M.: Super-twisting sliding mode controller with self-tuning adaptive gains, European Journal of Control, 68, 100 690, available online 13 June 2022, 2022.

Moldenhauer, R. H. and Schmid, R.: Lidar-assisted nonlinear output regulation of wind turbines for fatigue load reduction, Wind Energy Science, 10, 1907–1928, 2025.

Pan, L., Xiong, Y., Zhu, Z., and Wang, L.: Research on variable pitch control strategy of direct-driven offshore wind turbine using KELM wind speed soft sensor, Renewable Energy, 184, 1002–1017, 2022.

Plestan, F., Shtessel, Y., Brégeault, V., and Poznyak, A.: New methodologies for adaptive sliding mode control, International Journal of Control, 83, 1907–1919, 2010.

Robertson, A., Jonkman, J., Masciola, M., Song, H., Goupee, A., Coulling, A., and Luan, C.: Definition of the semisubmersible floating system for phase II of OC4, Tech. rep., National Renewable Energy Lab.(NREL), Golden, CO (United States), 2014.

Sarbandi, M., Shahir, M. M., Hamida, M. A., and Plestan, F.: Robust Control for Floating Wind Turbines Using Adaptive Super-Twisting Algorithm in Region III, in: 2025 33rd Mediterranean Conference on Control and Automation (MED), pp. 1–6, Tangier, Morocco, 2025.

Shtessel, Y., Edwards, C., Fridman, L., and Levant, A.: Sliding Mode Control and Observation, Birkhäuser, New York, NY, USA, ISBN 978-0-8176-4892-3, 2014.

Shu, Z., Li, Q., He, Y., and Chan, P.: Observations of offshore wind characteristics by Doppler-LiDAR for wind energy applications, Applied Energy, 169, 150–163, 2016.

Sierra-García, J. E. and Santos, M.: Improving wind turbine pitch control by effective wind neuro-estimators, IEEE Access, 9, 10 413–10 425, 2021.

Soltani, M. N., Knudsen, T., Svenstrup, M., Wisniewski, R., Brath, P., Ortega, R., and Johnson, K.: Estimation of Rotor Effective Wind Speed: A Comparison, IEEE Transactions on Control Systems Technology, 21, 1155–1167, 2013.

https://doi.org/10.5194/wes-2025-206
Preprint. Discussion started: 21 November 2025
© Author(s) 2025. CC BY 4.0 License.

Song, D., Yang, J., Cai, Z., Dong, M., Su, M., and Wang, Y.: Wind estimation with a non-standard extended Kalman filter and its application on maximum power extraction for variable speed wind turbines, Applied Energy, 190, 670–685, 2017.

Stockhouse, D., Phadnis, M., Henry, A., Abbas, N. J., Sinner, M., Pusch, M., and Pao, L. Y.: A tutorial on the control of floating offshore wind turbines: Stability challenges and opportunities for power capture, IEEE Control Systems, 44, 28–57, 2024.

Zhang, Y., Kong, X., Wang, J., Wang, S., Zhao, Z., and Wang, F.: A comprehensive wind speed prediction system based on intelligent optimized deep neural network and error analysis, Engineering Applications of Artificial Intelligence, 128, 107 479, 2024.